

Competition between excitation and emission enhancements of quantum dots on disordered plasmonic nanostructures

Seung Ho Choi,¹ Bongseop Kwak,² Bumsoo Han,² and Young L. Kim^{1,*}

¹Weldon School of Biomedical Engineering, Purdue University, West Lafayette, Indiana 47907, USA

²School of Mechanical Engineering, Purdue University, West Lafayette, Indiana 47907, USA

*youngkim@purdue.edu

Abstract: Plasmon-enhanced fluorescence is attributable to two independent processes: 1) excitation enhancement due to an increased electric field near metallic nanostructures and 2) emission enhancement from a surface plasmon resonance-coupled excited state of fluorophores. Using semiconductor nanocrystals (quantum dots) on disordered plasmonic nanostructures and a mesoscopic imaging approach, we demonstrate that increased excitation can diminish the fluorescence emission enhancement efficiency. Thus, our experimental evidence on this competitive behavior has critical implications for better developing plasmon-enhanced photoluminescence.

©2012 Optical Society of America

OCIS codes: (250.5403) Plasmonics; (300.6280) Spectroscopy, fluorescence and luminescence; (100.2980) Image enhancement; (220.4241) Nanostructure fabrication.

References and links

- Y. Chen, K. Munechika, and D. S. Ginger, "Dependence of fluorescence intensity on the spectral overlap between fluorophores and plasmon resonant single silver nanoparticles," *Nano Lett.* **7**(3), 690–696 (2007).
- P. Bharadwaj and L. Novotny, "Spectral dependence of single molecule fluorescence enhancement," *Opt. Express* **15**(21), 14266–14274 (2007).
- Y. Zhang, A. Dragan, and C. D. Geddes, "Wavelength dependence of metal-enhanced fluorescence," *J. Phys. Chem. C* **113**(28), 12095–12100 (2009).
- Y. C. Chen, K. Munechika, I. Jen-La Plante, A. M. Munro, S. E. Skrabalak, Y. N. Xia, and D. S. Ginger, "Excitation enhancement of CdSe quantum dots by single metal nanoparticles," *Appl. Phys. Lett.* **93**(5), 053106 (2008).
- K. Munechika, Y. Chen, A. F. Tillack, A. P. Kulkarni, I. J. Plante, A. M. Munro, and D. S. Ginger, "Spectral control of plasmonic emission enhancement from quantum dots near single silver nanoprisms," *Nano Lett.* **10**(7), 2598–2603 (2010).
- V. I. Klimov, ed., *Semiconductor and Metal Nanocrystals* (CRC Press, 2003).
- D. Tonti, F. van Mourik, and M. Chergui, "On the excitation wavelength dependence of the luminescence yield of colloidal CdSe quantum dots," *Nano Lett.* **4**(12), 2483–2487 (2004).
- Z. Xu, X. Sun, J. Liu, Q. Song, M. Muckley, O. Akkus, and Y. L. Kim, "Spectroscopic visualization of nanoscale deformation in bone: interaction of light with partially disordered nanostructure," *J. Biomed. Opt.* **15**(6), 060503 (2010).
- Z. Xu, J. Liu, D. H. Hong, V. Q. Nguyen, M. R. Kim, S. I. Mohammed, and Y. L. Kim, "Back-directional gated spectroscopic imaging for diffuse light suppression in high anisotropic media and its preclinical applications for microvascular imaging," *IEEE J. Sel. Top. Quantum Electron.* **16**(4), 815–823 (2010).
- Y. L. Kim, J. Liu, R. K. Wali, H. K. Roy, M. J. Goldberg, A. K. Kromin, K. Chen, and V. Backman, "Simultaneous measurement of angular and spectral properties of light scattering for characterization of tissue microarchitecture and its alteration in early precancer," *IEEE J. Sel. Top. Quantum Electron.* **9**(2), 243–256 (2003).
- P. Anger, P. Bharadwaj, and L. Novotny, "Enhancement and quenching of single-molecule fluorescence," *Phys. Rev. Lett.* **96**(11), 113002 (2006).
- L. N. Xu, B. J. Lee, W. L. Hanson, and B. Han, "Brownian motion induced dynamic near-field interaction between quantum dots and plasmonic nanoparticles in aqueous medium," *Appl. Phys. Lett.* **96**(17), 174101 (2010).
- E. Dulkeith, M. Ringler, T. A. Klar, J. Feldmann, A. Muñoz Javier, and W. J. Parak, "Gold nanoparticles quench fluorescence by phase induced radiative rate suppression," *Nano Lett.* **5**(4), 585–589 (2005).

14. J. Kim, G. Dantelle, A. Revaux, M. Bérard, A. Huignard, T. Gacoin, and J. P. Boilot, "Plasmon-induced modification of fluorescent thin film emission nearby gold nanoparticle monolayers," *Langmuir* **26**(11), 8842–8849 (2010).
15. <http://www.horiba.com/scientific/products/fluorescence-spectroscopy/application-notes/quantum-yields>
16. F. Tam, G. P. Goodrich, B. R. Johnson, and N. J. Halas, "Plasmonic enhancement of molecular fluorescence," *Nano Lett.* **7**(2), 496–501 (2007).
17. C. Sönichsen, T. Franzl, T. Wilk, G. von Plessen, J. Feldmann, O. Wilson, and P. Mulvaney, "Drastic reduction of plasmon damping in gold nanorods," *Phys. Rev. Lett.* **88**(7), 077402 (2002).
18. J. H. Song, T. Atay, S. F. Shi, H. Urabe, and A. V. Nurmikko, "Large enhancement of fluorescence efficiency from CdSe/ZnS quantum dots induced by resonant coupling to spatially controlled surface plasmons," *Nano Lett.* **5**(8), 1557–1561 (2005).
19. D. E. Gómez, K. C. Vernon, P. Mulvaney, and T. J. Davis, "Surface plasmon mediated strong exciton-photon coupling in semiconductor nanocrystals," *Nano Lett.* **10**(1), 274–278 (2010).
20. W. Jacak, J. Krasnyj, J. Jacak, W. Donderowicz, and L. Jacak, "Mechanism of plasmon-mediated enhancement of photovoltaic efficiency," *J. Phys. D Appl. Phys.* **44**(5), 055301 (2011).
21. S. M. Sadeghi, R. G. West, and A. Nejat, "Photo-induced suppression of plasmonic emission enhancement of CdSe/ZnS quantum dots," *Nanotechnology* **22**(40), 405202 (2011).

1. Introduction

Localized surface plasmon resonance-enhanced fluorescence (LSPReF) has received considerable attentions in numerous applications and research areas. While the primary utilization has been in biomolecule detections as biosensors, LSPReF has also played an important role in LEDs, photovoltaics, and photoelectrochemical reactions. As one critical condition for maximizing LSPReF, plasmonic bands of metallic nanostructures are required to overlap with the emission and/or excitation bands of fluorophores [1–3]. When common organic dye molecules are used as fluorophores, the emission and excitation wavelengths of the fluorophores are typically overlapped. Thus, the excitation (or absorption) enhancement and the emission enhancement are coupled together. Slight spectral offsets, which are often required to achieve the strongest enhancement, may originate from the overlapping of excitation and emission bands of organic fluorophores [1–3].

To decouple the excitation and emission enhancements, semiconductor nanocrystals, as known as quantum dots (QDs), have successfully been used [4,5]. Using QDs, the effects of the scattering cross-sections of metallic nanostructures on the excitation and emission enhancements have been investigated [4,5]. In particular, the recent studies using QDs near single silver nanoprisms showed that the fluorescence enhancement is proportional to the scattering cross-section of metallic nanostructures at either excitation and/or emission wavelengths of QDs [4,5]. Overall, these results support the idea that LSPReF can be enhanced by either matching the spectral bands or increasing the scattering power of metallic nanostructures.

As QDs are typically made from II/VI and III/V semiconductors, commercially available QDs consist of a semiconductor core (e.g. CdSe or CdTe) and a semiconductor shell (e.g. ZnS). QDs have extended electronic orbitals that have high energy levels to form the conduction band and photoluminescence of QDs originates from radiative exciton annihilation (i.e. electron-hole bound state) in competition with another nonradiative decay processes [6]. The properties of QDs can provide several advantages for LSPReF: 1) QDs can be excited at a low wavelength to avoid the spectral overlap with the emission band, if the excitation energy is higher than the bandgap energy. 2) The emission bands are significantly narrower than those of organic dyes, allowing the utilization of several different emission QDs simultaneously. 3) The intrinsic quantum yield of QDs is independent of the excitation wavelength [7]. On the other hand, LSPReF using QDs could potentially be sophisticated, because of interactions between the surface plasmons and the semiconductor properties of QDs. Indeed, this potential coupling effect on LSPReF in QD plasmonic systems has not yet been intensively investigated, to the best of our knowledge, although QDs on plasmonic nanostructures are actively used for numerous studies and applications of plasmon-enhanced photoluminescence.

Here, we report the first experimental evidence that an increase in the scattering intensity from metallic nanostructures at the excitation wavelength of QDs can reduce the fluorescence

emission enhancement efficiency. In other words, we demonstrate a competition between excitation and emission enhancements from QDs near plasmonic nanostructures. To investigate this intriguing characteristic of LSPReF, we have conducted the following studies: 1) We fabricated disordered metallic nanostructures to obtain a variety of combinations of reflectance intensities from metallic nanostructures at the excitation and emission bands of QDs. 2) Using our new-developed mesoscopic (i.e. between microscopic and macroscopic) spectroscopic imaging setup, we characterized reflectance and emission spectra in a relatively large area, generating a significant number of data points. 3) We statistically analyzed the emission enhancement efficacy of QDs as functions of the reflectance intensities of the metallic nanostructures.

2. Methods

We first fabricated simple plasmonic nanostructures by self-assembling colloidal gold (Au) nanoparticles into disordered metallic nanostructures in different sizes. In particular, this approach was useful for achieving a variety of combinations of reflectance intensities from the Au nanostructures at the excitation and/or emission bands of QDs. Figure 1(a) illustrates

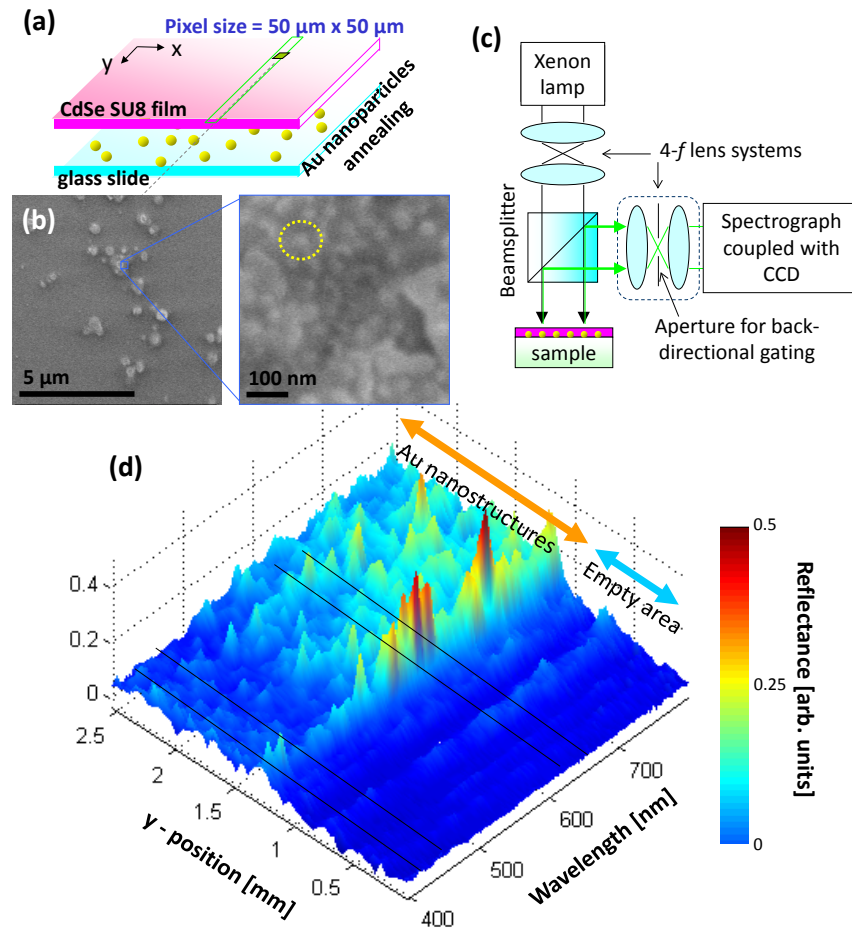


Fig. 1. (a) Schematic of the fabrication procedure of QD-embedded SU8 on the disordered Au nanostructures. (b) (Left) Representative SEM image of self-assembled Au clusters in an area similar to the optical imaging pixel. (Right) 50-nm Au nanoparticles can be seen in individual Au clusters. (c) Schematic of our mesoscopic spectroscopic imaging setup of capable of imaging a relative large area with a small cone of backscattering angle via back-directional gating. (d) Typical reflectance spectra from the Au nanostructures before QD-embedded SU8 is spin-coated, along a line as illustrated in (a).

the fabrication procedure. In brief, colloidal Au nanoparticles with a mean diameter of 50 nm (BBI International) were dropped on a glass substrate (i.e. microscope slide) covering an area of ~ 15 mm \times 15 mm. The Au nanoparticles were self-assembled and during an annealing procedure at 300 °C for 10 min, heterogeneous nanostructures were formed. Then, QD-embedded SU8 were coated on the top of the nanostructures. We used QDs with emission at 655 nm (Invitrogen, Qtracker® 655 Non-Targeted Quantum Dots). QDs and a prepolymer of SU8 were mixed at a ratio of 1:20 and this mixture was spin-coated at a speed of 1200 rpm, which produced a uniform layer with a thickness of 1 μm . Figure 1(b) shows a representative scanning electron microscopy (SEM) image in an area similar to the pixel size of our optical imaging setup. As shown in Fig. 1(b), the Au nanostructures were assembled by individual 50-nm gold particles. The SEM images indicate that the Au clusters were relatively packed and randomly distributed in the size range from 50 nm to 1 μm .

To acquire spatial and spectral patterns of reflectance from the Au nanostructures and fluorescence from QDs, we utilized our recently developed mesoscopic imaging setup [8,9], as shown in Fig. 1(c). This mesoscopic imaging system is based on the combination of back-directional angle gating and spectral imaging: 1) Back-directional gating in the detection part allows us to collect the light scattered and emitted from the specimen in the exact back direction with a small cone of angle of $\sim 5^\circ$. This fixed detection geometry is beneficial for obtaining consistent reflectance signals in a relatively large area. 2) This system provides a matrix of intensity as a function of x and y at each wavelength λ in the range of 400 – 800 nm. The imaging area of our mesoscopic imaging setup was ~ 15 mm \times 15 mm with a pixel size of 50 $\mu\text{m} \times$ 50 μm . In our experiments, the large field of view of our mesoscopic imaging system generated $\sim 90,000$ ($= 300 \times 300$) reflectance spectra consisting of different intensities at 430 nm and 655 nm, which corresponded to the excitation and emission wavelengths of QDs, respectively. Figure 1(d) shows typical reflectance spectra from the fabricated Au nanostructures along the line illustrated in Fig. 1(a).

3. Results

To gain a better understanding of the Au nanostructures and the origin of the multiple peaks in the reflectance spectra (Fig. 1(d)), we further utilized SEM image and Mie calculations. Several different size Au clusters were attributable to the reflectance spectrum in each imaging pixel. In Fig. 2(a), we selected two representative Au nanostructure clusters: Cluster type A consisting of one large subcluster and two small subclusters and Cluster type B consisting of three middle sized subclusters. Assuming that the effect of inter-cluster correlations was minimal, we calculated the scattering cross-section of Au nanoparticles using Mie calculations [10]. Figure 2(b) illustrates that the resulting reflectance spectra of the fabricated Au nanostructure can qualitatively be understood to be the superposition of individual Au clusters in different sizes, although the resulting clusters were not completely sphere-shaped. Thus, it is likely that the different sizes of subclusters were responsible to the multiple resonance peaks (Fig. 1(d)). As a result, as shown in Fig. 2(c), our Au nanostructures provided the variety of combination of reflectance intensities at 430 nm and 655 nm, which served as the foundation for our data analyses. Indeed, when we further visualized reflectance images at 430 nm and 655 nm of representative Au nanostructures (before QD-embedded SU8 was coated on top), the reflectance image at 430 nm (Fig. 2(d)) was different from the reflectance image at 655 nm (Fig. 2(e)).

To perform fluorescence measurements after QD-embedded SU8 was coated on the top of the Au nanostructures, a narrow bandpass filter at 430 ± 15 nm for excitation illumination was added in the delivery part of the imaging setup (Fig. 1(c)) and QD emission was acquired. This system also allowed us to measure precise fluorescent emission intensities by obtaining the emission spectrum at each (x , y) location. The plasmonic fluorescence emission enhancement factor E was defined as the ratio of the fluorescence intensity of QDs integrated within 655 ± 15 nm in the areas of the Au nanostructures ($= I_{\text{FL}}$) to that in the areas without the Au nanostructures (background $= I_0^{\text{FL}}$):

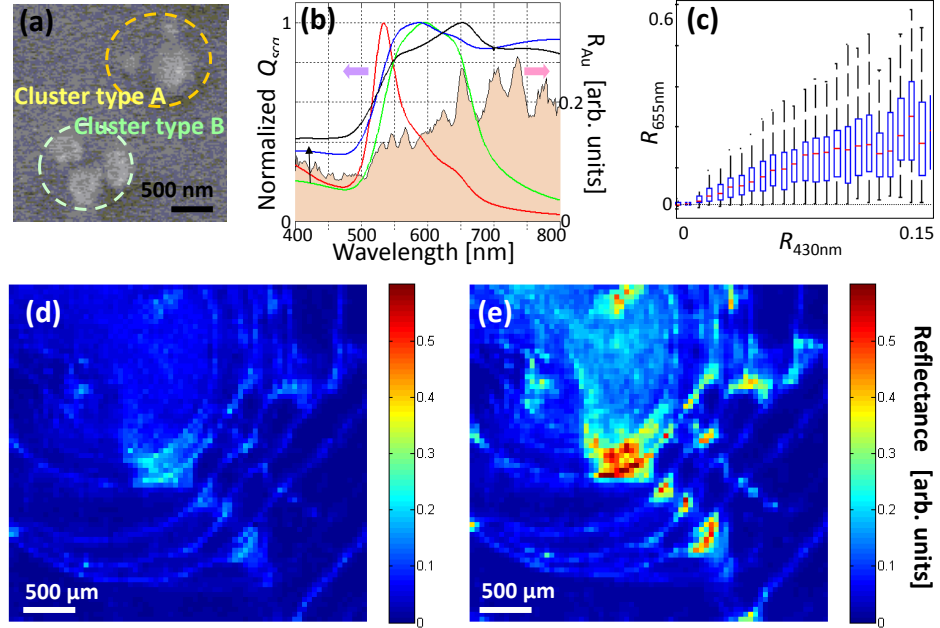


Fig. 2. (a) SEM of typical Au nanoparticle clusters. Different sizes of Au clusters are closed positioned among others. (b) Calculated scattering cross-sections Q_{sca} of single Au nanospheres (diameter = 50, 100, 300, and 500 nm) using Mie calculations and representative reflectance spectrum of the Au nanostructures (shaded area curve). The multiple peaks in the Au reflectance spectrum can be considered to be the superposition of Au clusters in different sizes. (c) The intensity distribution of the reflectance from the Au structures at 430 nm (= $R_{430\text{nm}}$) over the reflectance from the Au structures at 655 nm (= $R_{655\text{nm}}$). Such a large data set allows us to statistically investigate the effects of Au reflectance intensities at the excitation and emission bands of QDs. On the each box, the central mark is the median and the edges of the box are the 25th and 75th percentiles. (d) and (e) Visualization of representative reflectance images of the Au nanostructures without QD-embedded SU8 at 430 nm and 655 nm, respectively.

$$E = \frac{I^{FL}}{I_0^{FL}} \quad (1)$$

Figure 3(a) shows that in general E was higher in the pixels where the Au nanostructures were placed.

We further visualized the details of E of QDs as a function of the reflectance intensities of the Au nanostructures (before QD-embedded SU8 was coated) at 430 nm and 655 nm. We integrated the reflectance intensity at 430 nm (= $R_{430\text{nm}}$), the reflectance intensity at 655 nm (= $R_{655\text{nm}}$), and E . In Fig. 3(b), the x - and y -axes are $R_{430\text{nm}}$ and $R_{655\text{nm}}$, respectively, while E is visualized in different color at each data point. As expected, E increases with $R_{430\text{nm}}$ or $R_{655\text{nm}}$. We also note that E was in a relatively low range from 1 to 3 in our QD-Au nanostructure system. As a near-field effect, typical distances between fluorophores and metallic surface for LSPReF are $\sim 5 - 100$ nm [[1,5,11-14]]. Because the thickness of QD-embedded SU8 was ~ 1 μm, QDs located beyond the typical distance must have generated the strong baseline fluorescence intensity, without contributing to LSPReF.

We also measured the intrinsic quantum yield of QDs in the absence of Au nanostructures using two standard references with the known quantum yield values [15], because the intrinsic quantum yield sets a limit for LSPReF. For example, E decreases as the quantum yield reaches to 100% [5,11]. In other words, in any fluorophores with a quantum yield of 100%, fluorescence emission cannot be enhanced anymore. Our measurement showed that the intrinsic quantum yield of QDs was 50%. Thus, it is highly unlikely that the relatively low

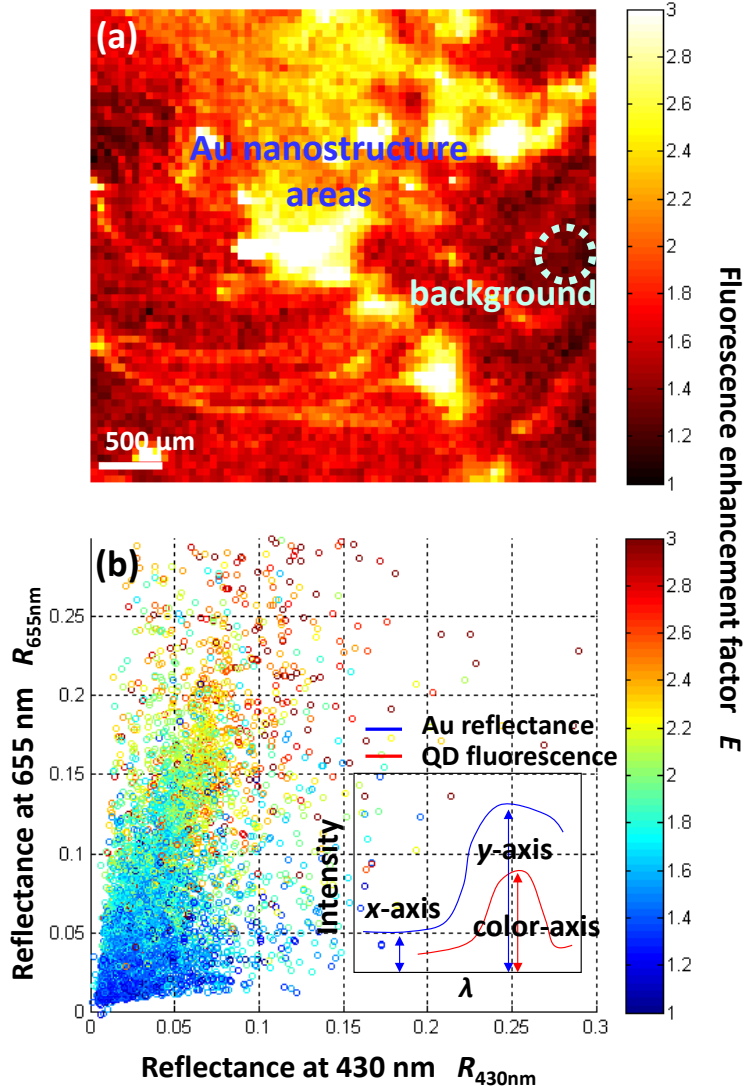


Fig. 3. (a) Visualization of the plasmonic fluorescence enhancement factor E after QD-doped SU8 is spin-coated on the top of the Au nanostructures. (b) Plot using the reflectance data at 430 nm $R_{430\text{nm}}$, the reflectance image at 655 nm $R_{655\text{nm}}$, and the fluorescence enhancement factor E . The x - and y -axes are $R_{430\text{nm}}$ and $R_{655\text{nm}}$, while E is visualized in different colors at each data point. Inset: Illustration of the origins of the data set. $R_{430\text{nm}}$ and $R_{655\text{nm}}$ are obtained from the Au reflectance intensities (before the coating of QD-embedded SU8) at the different wavelengths λ , while E is obtained from the emission spectra after the coating of QD-embedded SU8 at 655 nm.

value of E was a manifestation of LSPReF originating from an extremely high quantum yield of QDs.

We further explored how E varies as $R_{655\text{nm}}$ increases at a given $R_{430\text{nm}}$ as shown in Fig. 4. In particular, we defined the emission enhancement efficiency β_{em} as the linear slope of E over $R_{655\text{nm}}$ at a given $R_{430\text{nm}}$ such that

$$\beta_{em} = \frac{dE}{dR_{655\text{nm}}}. \quad (2)$$

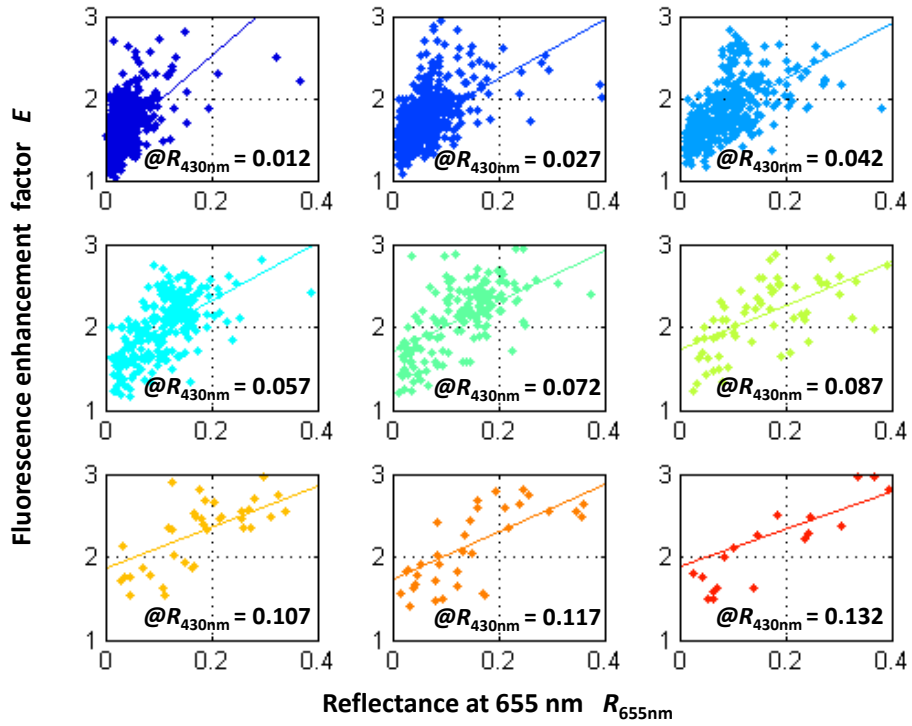


Fig. 4. Changes in E as $R_{655\text{nm}}$ increases at different $R_{430\text{nm}}$. Each data set at different $R_{430\text{nm}}$ can be captured as a linear relationship between E and $R_{655\text{nm}}$. In each panel, the emission enhancement efficiency β_{em} is defined as the slope in each linear fit. The excitation enhancement factor α_{ex} is defined as the y -intercept, because it corresponds to a value of E when $R_{655\text{nm}} = 0$.

In addition, the vertical intercept of each linear line at a given $R_{430\text{nm}}$ provides the baseline enhancement mainly originated from the excitation enhancement without the contribution of $R_{655\text{nm}}$. The intercept of each linear fit can be referred to as the excitation enhancement factor α_{ex} . Thus, the overall relationship between E and $R_{655\text{nm}}$ at a fixed $R_{430\text{nm}}$ can be expressed such that

$$E = \alpha_{ex} + \beta_{em} R_{655\text{nm}}. \quad (3)$$

Surprisingly, Fig. 5(a) reveals that when we plot β_{em} (i.e. slopes of linear fits in Fig. 4) over $R_{430\text{nm}}$, β_{em} decreases with $R_{430\text{nm}}$. This result clearly demonstrates that a competition mechanism exists between the excitation enhancement and the emission enhancement in our QD-Au plasmonic system. In other words, the enhanced absorption for QDs induced by the high scattering cross-section of $R_{430\text{nm}}$ can lower β_{em} . Because the P-value of the slope estimate of the linear regression between β_{em} and $R_{430\text{nm}}$ is 0, the null hypothesis that the slope is zero can be rejected. Thus, the negative association between β_{em} and $R_{430\text{nm}}$ is statistically significant. On the other hand, Fig. 5(b) shows that when we plot α_{ex} (i.e. vertical intercepts of the linear fits in Fig. 4) over $R_{430\text{nm}}$, α_{ex} linearly increases with $R_{430\text{nm}}$. The P-value of the slope estimate of the linear regression between α_{ex} and $R_{430\text{nm}}$ is 0 and thus, the association is also statistically significant. Indeed, the latter result agrees with the previous studies that the fluorescence enhancement is proportional to the scattering cross-section of metallic nanostructures [[4,5,16]]. Overall, our results reveal that the effects of the scattering cross-section of metallic nanostructures on the emission enhancements of QDs can be distinct, compared with LSPReF using organic dyes.

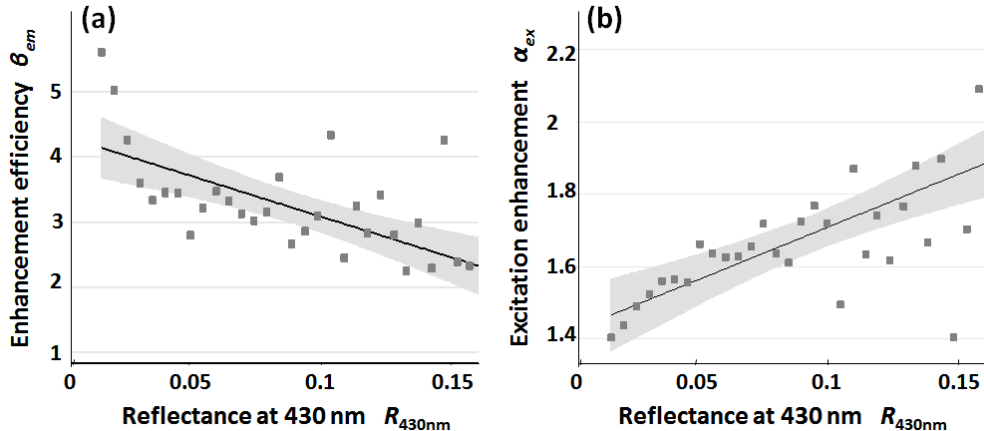


Fig. 5. (a) Correlation of the emission enhancement efficiency β_{em} with R_{430nm} . The negative linear correlation coefficient reveals that the fluorescence emission rate is reduced by the enhanced excitation (or absorption) at 430 nm, indicating a competitive coupling between the excitation and emission enhancements in QD plasmonic systems. The gray band in the graph shows the 95% confidence intervals of the expected β_{em} . (b) Correlation of the excitation enhancement factor α_{ex} with R_{430nm} . The gray band in the graph shows the 95% confidence intervals of the expected α_{ex} . E linearly increases with the enhanced excitation (or absorption) at 430 nm when $R_{655nm} = 0$, which is in good agreement with the previous results that E is linearly proportional to the scattering cross-section of metallic nanostructures [4,5].

4. Discussion

Our experimental results above are unexpected in the context of the current understanding of LSPReF, in which the enhanced absorption of fluorophores at the excitation wavelength does not modulate the coupling of the fluorophores with LSPR at the emission wavelength. Conventional LSPReF can be understood on two basic mechanisms [1,5,11–14]: 1) An increased electric field in the vicinity of metallic nanostructures, such as nanoparticles, enhances the absorption of fluorophores (i.e. excitation enhancement) and 2) the excited state of fluorophores is coupled with LSPR (i.e. emission enhancement or quenching). Thus, E can be expressed such that

$$E = \frac{\gamma_{ex}}{\gamma_{ex}^0}(\lambda_{ex}) \frac{q}{q^0}(\lambda_{em}), \quad (4)$$

where γ_{ex} is the excitation rate, γ_{ex}^0 is the corresponding excitation rate in free space, q is the quantum yield of spontaneous emission coupled into LSPR, q^0 is the corresponding quantum yield in free space, λ_{ex} is the excitation wavelength, and λ_{em} is the emission wavelength of fluorophores. The excitation enhancement term ($= \gamma_{ex}/\gamma_{ex}^0$) is independent of the emission enhancement term ($= q/q^0$). On the other hand, our experimental results (Fig. 5(a)) clearly show that the excitation enhancement can reduce the emission enhancement efficacy.

While our current studies do not attempt to address detailed mechanisms of the competition between the excitation and emission enhancements of the QD-Au plasmonic system, the potential mechanism could be postulated as follows: 1) One possibility could potentially be damping of LSPR induced by the near-field coupling with the interband transition in QDs [17–20]. When the excitation field excites the excitons in QDs and the surface plasmons in metallic nanostructures, the excitons can transfer the energy into radiative and nonradiative surface plasmon polaritons. If the surface plasmon polaritons are coupled with the exciton transition in QDs, strongly and weakly coupled cases can occur, depending on the degrees of exciton-plasmon coupling and dephasing of exciton or plasmon resonance. In particular, in a weakly coupled case, surface plasmons from metallic nanostructures could

damp exciton-plasmon coupling and thus reduce the radiative decay rate of the exciton state in QDs. 2) Another possibility could potentially originate from photoionization and Coulomb blockades of QDs, although these effect are primarily related with photo-induced fluorescence enhancement of QDs [6], in which QD emission is enhanced by light irradiation. The energy transfer between QDs and metallic nanostructures via the plasmonic field could suppress the Coulomb blocking due to photoionization of QDs, suppressing plasmonic emission enhancement [21]. Future studies are required to understand detailed underlying mechanisms of the decreased emission enhancement efficiency of QDs. We expect that our experimental evidence will serve as the first step to stimulate more theoretical work.

Given that the unique optical properties of QDs have been the object of intensive investigation, our current studies can serve as unique models for better understanding plasmon-enhanced photoluminescence of QDs. Indeed, a quantitative understanding of the excitation and emission enhancements in LSPR-enhanced QD systems is critical for a variety of applications ranging from plasmon-enhanced photoluminescence, photovoltaics, to photoelectrochemical reactions, all of which have several implications ranging from sensing to directed energy. For example, LED applications often require increasing radiative rates without enhancing excitation, whereas solar cell development can be facilitated by maximizing the excitation enhancement. In addition, the advantage of our nanostructure fabrication is that it can easily be fabricated under common laboratory conditions, without requiring advanced nanofabrication methods. Thanks to the disordered nanostructures, we could avoid intensive specimen fabrications to form different nanostructures. Whereas most studies in nanosciences and nanotechnologies rely on high-resolution microscopic methods, our studies also demonstrate that our mesoscopic approach is useful. Consequently, the combination of the simple nanostructure fabrication and the mesoscopic imaging system allowed us to perform a systematic study of LSPReF in the QD-Au plasmonic system.

5. Conclusion

We demonstrate that an increase in the reflectance intensity of metallic nanostructures can reduce the fluorescence emission enhancement efficiency of QDs. To the best of our knowledge, this is the first experimental evidence to show a competition between excitation and emission enhancements in QDs near plasmonic nanostructures. Because conventional frameworks in LSPReF using organic dyes do not include this interaction, we expect that our experimental demonstration will facilitate more theoretical studies to elucidate detailed mechanisms of the competition between the excitation and emission enhancements of QD-metallic nanostructure systems. In addition, a better understanding of this competitive characteristic of LSPReF will be critical in various plasmon-enhanced photoluminescence applications using QDs.

Acknowledgments

We acknowledge the generous support from the Abbott Laboratories and thank Zhengbin Xu for help with the imaging setup.